Journal of Materials Chemistry A

RSC Publishing

PAPER

View Article Online
View Journal | View Issue

Cite this: J. Mater. Chem. A, 2013, 1, 9928

Synthesis of polypropylene/Mg_3Al–X (X = CO_3^{2-}, NO_3^-, Cl^-, SO_4^{2-}) LDH nanocomposites using a solvent mixing method: thermal and melt rheological properties

Yanshan Gao,[a] Jingwen Wu,[a] Zhang Zhang,[a] Rong Jin,[a] Xi Zhang,[b] Xingru Yan,[b] Ahmad Umar,[cd] Zhanhu Guo[b] and Qiang Wang*[a]

Received 30th April 2013
Accepted 24th June 2013

DOI: 10.1039/c3ta11695f

www.rsc.org/MaterialsA

In this contribution, polypropylene (PP) nanocomposites with four different inorganic anion (CO_3^{2-}, NO_3^-, Cl^-, and SO_4^{2-}) intercalated Mg_3Al layered double hydroxides (LDHs) as nanofillers were prepared using a solvent mixing method for the first time. The influence of interlayer inorganic anions on the thermal stability, melting and recrystallisation behavior and rheological property of PP was then systematically compared. The thermal stability was significantly improved, with Mg_3Al–CO_3 and Mg_3Al–Cl LDHs, and $T_{0.5}$ increased by about 44 °C compared to pure PP. The incorporation of LDHs increased the melting temperature (T_m) and the recrystallization temperature (T_c) of PP by about 3–4 °C and 10–13 °C, respectively. The influence on the storage modulus (G') and loss modulus (G'') follows the order of Mg_3Al–SO_4 > Mg_3Al–NO_3 > Mg_3Al–CO_3 > Mg_3Al–Cl. Although the incorporation of all LDHs led to an improvement in the thermal stability, T_m, T_c, G', G'', and complex viscosity of PP/Mg_3Al–X LDH nanocomposites, the extent of changes varied with the type of inter-layer anions. The study finally demonstrated that even very similar inorganic anions such as CO_3^{2-}, NO_3^-, Cl^-, and SO_4^{2-} could lead to a significant difference in the property of the synthesized PP/LDH nanocomposites, and it must be taken into account for the future design of polymer/LDH nanocomposites.

1 Introduction

Polymer nanocomposites have received much attention due to their potential wide applications such as electronic devices,[1] membranes,[2,3] solar cells,[4] microwave absorption,[5,6] electrochromic devices,[7] and structural materials arising from their unique physicochemical properties, which are superior to the conventional composites with the filler size larger than 100 nm.[8–10] Polypropylene (PP) is one of the most widely used commodity thermoplastics, which has excellent physical properties, such as high stiffness and tensile strength.[11,12] PP has been widely used in cables, household appliances, food packaging, automotive components, and medical devices.[9] However, it has a low thermostability and is a kind of flammable material. Therefore, in order to improve its thermostability and flame retardancy, generally some nanofillers are added to the PP matrix to prepare nanocomposites.

In recent years, polymer/LDH nanocomposites have attracted considerable attention in the field of materials chemistry. LDHs are a class of ionic lamellar compounds made up of positively charged brucite-like layers with an interlayer region containing charge compensating anions and solvation molecules.[13,14] The LDH materials have received increasing attention due to their many applications as precursors to CO_2 adsorbents,[15–19] catalysts,[20,21] thermal stabilizers,[22,23] IR absorbers,[24,25] UV absorbers,[26–28] and nanofillers in polymer/LDH nanocomposites.[29–33] The major advantage of LDHs is that they are synthetic materials in which the chemical composition of both the inorganic layers and the interlayer gallery anions can be varied. This gives LDHs highly tunable properties and makes them promising materials widely used in the above fields. Until now, many kinds of LDHs have been reported as nanofillers in polymer/LDH nanocomposites. For instance, LDHs with different cationic compositions such as Mg–Al,[30,34,35] Zn–Al,[36,37] and Mg–Zn–Al LDHs[38,39] have been proven to be good flame retardant materials, in the meantime, both the thermal stability and rheological properties can be enhanced as well.

Because of the intrinsic hydrophilic nature of LDHs, they generally do not exhibit native compatibility with non-polar polyolefin hosts (*e.g.* PP); currently most of the PP/LDH

[a]College of Environmental Science and Engineering, Beijing Forestry University, 35 Qinghua East Road, Haidian District, Beijing 100083, P. R. China. E-mail: qiang.wang.ox@gmail.com; qiangwang@bjfu.edu.cn; Tel: +86-13699130626

[b]Integrated Composites Laboratory, Dan F Smith Department of Chemical Engineering, Lamar University, Beaumont, TX 77710, USA

[c]Department of Chemistry, College of Science and Arts, Najran University, P.O. Box 1988, Najran-11001, Kingdom of Saudi Arabia

[d]Promising Centre for Sensors and Electronic Devices (PCSED), Najran University, P.O. Box 1988, Najran-11001, Kingdom of Saudi Arabia

nanocomposites are prepared using the melt mixing method, by which the polymer and dried LDH powders are mixed in an extruder at an elevated temperature. However, one problem is that the LDH nanoparticles aggregate severely when being dried, which can result in a poor dispersion of the LDH nanoparticles in the polymer matrix. Therefore, in order to make highly dispersed polymer/LDH nanocomposites, solvent mixing is preferred. In order to improve the compatibility between LDH and PP, one solution is to intercalate surfactant anions into the LDH inter-layers. Recently, we reported a new method that makes it possible to disperse inorganic anion intercalated LDHs in nonpolar solvents (*e.g.* xylene). Polymer/LDH nanocomposites can then be prepared by the solvent mixing method.[12]

Previously, since inorganic anion intercalated LDH–X (X = CO_3^{2-}, NO_3^-, Cl^-, and SO_4^{2-}) cannot be added into PP using the solvent mixing method, a systematic investigation on the influences of interlayer inorganic anions on the performance of PP/Mg_3Al–X LDH nanocomposites has not been performed. Therefore, in the present work, we will use the newly developed method to synthesize PP/Mg_3Al–X (X = CO_3^{2-}, NO_3^-, Cl^-, and SO_4^{2-}) LDH nanocomposites and systematically investigate their thermal stability, melting and recrystallisation behavior, and rheological property for the first time.

2 Experimental

2.1 Synthesis of LDHs and PP/LDH nanocomposites

Mg_3Al–X was synthesized by a traditional co-precipitation method. In brief, Mg_3Al–CO_3 LDH was prepared by adding a 50 ml solution containing 9.6 g Mg $(NO_3)_2 \cdot 6H_2O$ (0.0375 mol) and 4.7 g $Al(NO_3)_3 \cdot 9H_2O$ (0.0125 mol) drop-wise to a 50 ml solution containing 2.65 g Na_2CO_3 (0.025 mol). The pH of the precipitation solution was adjusted to *ca.* 10 using a NaOH (4 M) solution. Mg_3Al–NO_3, and Mg_3Al–SO_4 LDH can be synthesized in the same way, with an only exception that the Mg_3Al solution is added drop-wise to a 50 ml solution containing 2.125 g $NaNO_3$ (0.025 mol) or 3.55 g Na_2SO_4 (0.025 mol). Similarly, Mg_3Al_1–Cl was prepared by adding a $MgCl_2$ and $AlCl_3 \cdot xH_2O$ solution to a NaCl solution, with the pH adjusted to 10 using a NaOH solution. The obtained LDHs were washed with H_2O until pH = 7. The sample was further washed with acetone intensively. For the preparation of PP/LDH nanocomposites, the acetone washed slurries were directly used without drying. Finally all samples were dried in an oven at 65 °C overnight to obtain the LDH powders.

PP/Mg_3Al–X LDH nanocomposites were prepared using a solvent mixing method. 5 g of PP (molecular weight *ca.* 300 000), the acetone washed LDH slurry prepared above and 100 ml of xylene were charged into a 250 ml round bottom flask. The amount of LDH added to PP is 9 wt%. The mixture was refluxed at approximately 140 °C for 2 h. After the completion of the reflux process, the hot xylene solution containing the dissolved PP and highly dispersed LDH nanoparticles was poured into 100 ml hexane (also called the solvent extraction method). The obtained PP/LDH nanocomposites were collected by filtration and dried under vacuum.

2.2 Characterization of LDHs

XRD patterns were recorded on a PANalytical X'Pert Pro instrument in reflection mode with Cu Ka radiation. The accelerating voltage was set at 40 kV with 40 mA current (λ = 1.542 Å) at 0.01° s^{-1} from 1° to 70° with a slit size of 1/4 degree. TEM analysis was performed on a JEOL 2100 microscope with an accelerating voltage of 200 kV. Samples were dispersed in ethanol by sonication and then cast onto copper TEM grids coated with a lacey carbon film. SEM and SEM-EDX analyses were performed on a JEOL JSM 6100 scanning microscope with an accelerating voltage of 20 kV. Powder samples were spread on carbon tape adhered to a SEM stage. Before observation, the samples were sputter coated with a thin platinum layer to prevent charging and to improve the image quality.

2.3 Thermal stability and rheological property of PP/LDHs

The thermal stability of pure PP and its nanocomposites was studied by TGA (Netzsch), which was carried out at a heating rate of 10 °C min^{-1} and an air flow rate of 50 ml min^{-1} from 25 to 600 °C. The recrystallisation and melting behaviors of neat PP and nanocomposites were analysed using a TA Instrument Q200 differential scanning calorimeter (DSC). Experiments were run on samples of about 10 mg. Each sample was first heated from room temperature to 220 °C at a heating rate of 10 °C min^{-1} to remove the thermal history, cooled to 40 °C at a rate of 10 °C min^{-1}, and then reheated to 220 °C at a rate of 10 °C min^{-1} to determine the melting temperature. The experiments were carried out at a nitrogen flow rate of 50 ml min^{-1}. The melt rheological behavior of neat PP and the nanocomposites was studied using a TA Instruments AR 2000ex Rheometer. An environmental test chamber (ETC) steel parallel-plate geometry (25 mm in diameter) was used to perform the measurement at 200 °C, with the dynamic oscillation frequency sweeping from 100 to 0.1 Hz in the linear viscoelastic (LVE) range (strain 1%) under a nitrogen atmosphere to prevent the oxidation of PP.

3 Results and discussion

3.1 Characterization of LDHs

The synthesized Mg_3Al–X LDHs were first characterized using XRD analysis, as shown in Fig. 1. Six characteristic peaks which can be indexed to the reflections of (003), (006), (009), (015), (018), and (110/113) planes were observed for Mg_3Al–X LDHs, suggesting that all of the LDHs had a well-developed layer structure. A slight difference in the interlayer distance was observed when various anions were used, probably due to the difference in their dimension and carried charges. When CO_3^{2-} was inserted as a guest anion, the interlayer distance was ~7.80 Å, while when SO_4^{2-} was inserted, the distance expanded to 8.85 Å. The basal spacing values (d_{003}) follow the order of SO_4^{2-} (8.85 Å) > NO_3^- (8.80 Å) > Cl^- (8.04 Å) > CO_3^{2-} (7.80 Å), as shown in Fig. 1(b). Fig. 1 also shows the XRD patterns of Mg_3Al–NO_3 and Mg_3Al–CO_3 LDHs washed with acetone. It clearly shows that after Mg_3Al–NO_3 and Mg_3Al–CO_3 LDHs were further intensively washed with acetone, no significant changes

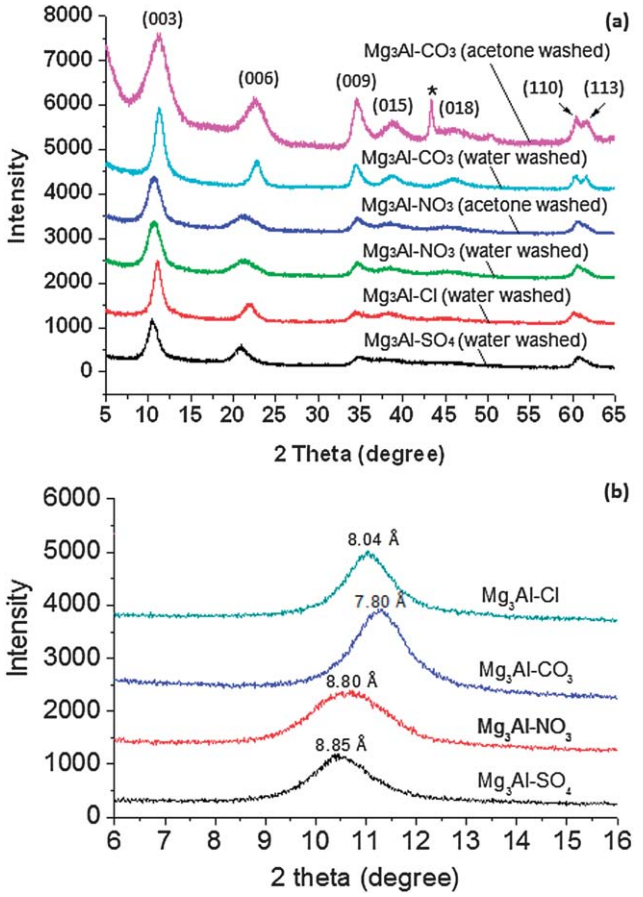

Fig. 1 (a) XRD patterns of Mg_3Al–X (X = CO_3^{2-}, NO_3^-, Cl^-, and SO_4^{2-}) LDHs washed with water and acetone, (★) sample holder. (b) XRD patterns of Mg_3Al–X (X = CO_3^{2-}, NO_3^-, Cl^-, and SO_4^{2-}) LDHs in the range of 6–16°.

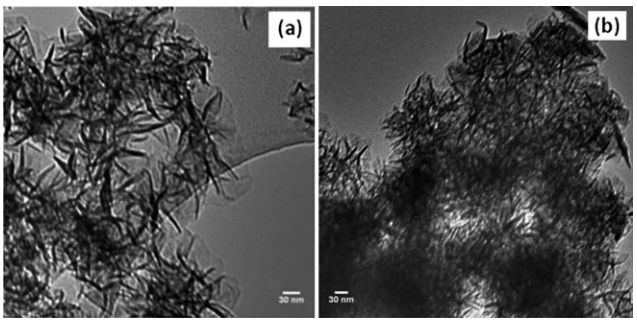

Fig. 2 TEM images of (a) Mg_3Al–NO_3 and (b) Mg_3Al–CO_3 LDHs.

in the XRD patterns were observed, suggesting that acetone treatment did not affect their layered structure.

TEM images of Mg_3Al–NO_3 and Mg_3Al–CO_3 LDHs are shown in Fig. 2. It is clear that both Mg_3Al–NO_3 and Mg_3Al–CO_3 LDH samples formed typical flower-like nanoparticles. Fig. 3 shows the SEM images of the dried powder of Mg_3Al–X LDHs, from which we can see that once the LDH nanoplates were separated from solution and dried to fine powders, they severely aggregated together. Both samples formed very big particles, with an average size of 0.1–0.2 μm. This clearly indicates that in order to

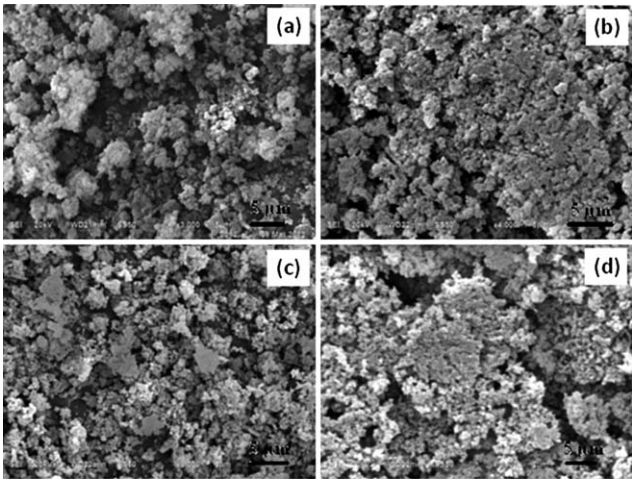

Fig. 3 SEM images of Mg_3Al–X LDHs, (a) Mg_3Al–CO_3 LDH, (b) Mg_3Al–NO_3 LDH, (c) Mg_3Al–Cl LDH, and (d) Mg_3Al–SO_4 LDH.

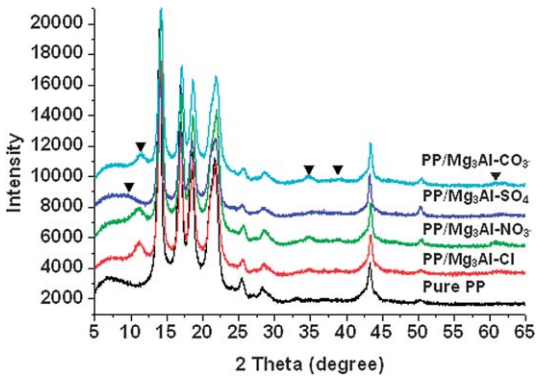

Fig. 4 XRD patterns of PP/Mg_3Al–X LDH nanocomposites with 9 wt% LDH loading and pure PP. (▼) Mg_3Al–X LDHs.

have a good dispersion of LDH nanosheets within the polymer matrix, LDH nanosheets should be introduced into polymers before any drying step. If the polymer/LDH nanocomposites were prepared using a melt mixing method from dried LDH powders, the dispersion of LDH would be much worse than that prepared using the solvent mixing method. Thus, in this contribution, we used a newly developed solvent mixing method for the preparation of PP/Mg_3Al–X LDH nanocomposites.

3.2 Characterization of PP/LDH nanocomposites

Fig. 4 shows the XRD patterns of pure PP and PP/Mg_3Al–X LDH nanocomposites with a loading of 9 wt%. The characteristic X-ray diffraction patterns of the LDH nanoparticles can be clearly seen, indicating that LDH nanoparticles were successfully introduced into PP.

The morphology of synthesized nanocomposites and the distribution of LDH nanoparticles were further examined by SEM analysis. Fig. 5 shows the SEM image of PP/Mg_3Al–CO_3 LDH nanocomposites with 9 wt% loading. Spherical particles with an average size of *ca.* 5 μm were formed. LDH particles can rarely be observed, which is due to the ultrafine LDH particles

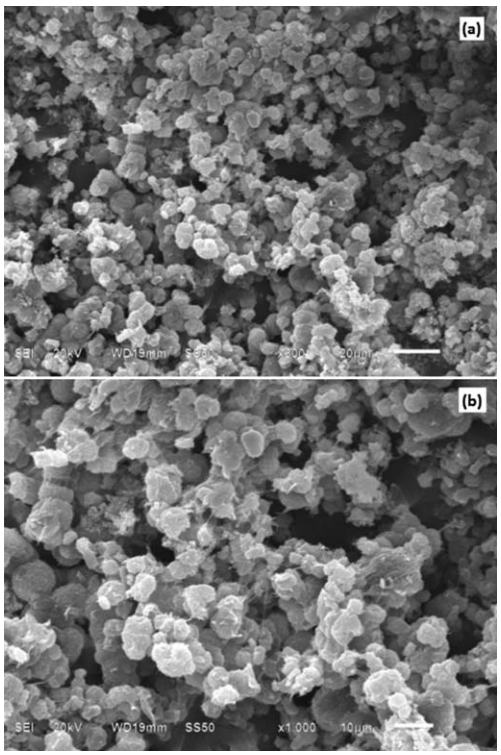

Fig. 5 SEM images of PP/Mg_3Al–CO_3 LDH nanocomposites with LDH loading of 9 wt%, (a) ×600 and (b) ×1000.

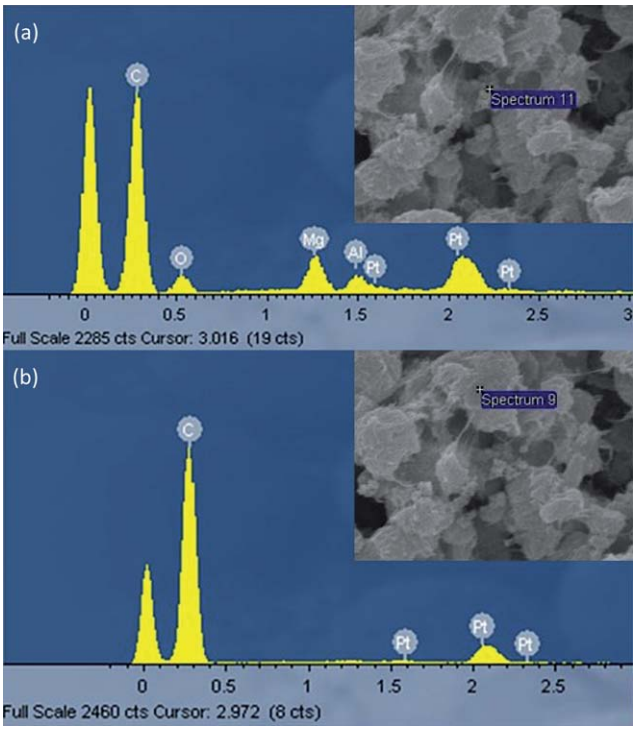

Fig. 6 SEM-EDX analysis of PP/Mg_3Al–CO_3 LDH nanocomposites. (a) EDX elemental analysis of the point representing LDH particles and (b) EDX elemental analysis of the point representing PP.

and their good dispersion within the PP matrix. There are few LDH-like nanoparticles seen on the surface. As a result, SEM-EDX was utilized to confirm that the surface nanoparticles are

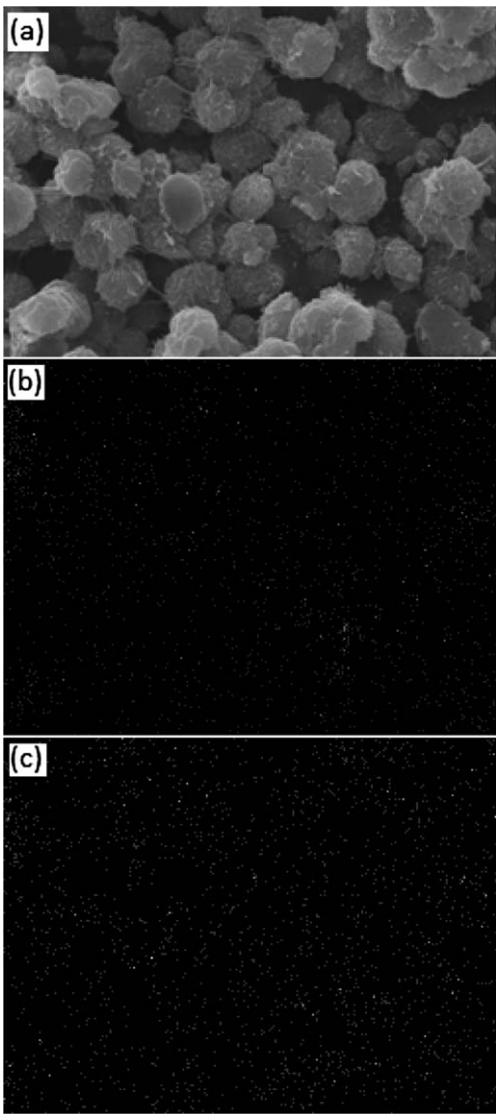

Fig. 7 (a) SEM image, (b) Mg mapping, and (c) Al mapping of 9 wt% PP/Mg_3Al–CO_3 nanocomposites.

Mg_3Al–CO_3 LDHs. The EDX elemental analysis of a representative surface nanoparticle is shown in Fig. 6. Fig. 6(a) and (b) show the EDX elemental analysis of the representative polymer surface and the LDH nanoparticle respectively. Mg and Al were detected in Fig. 6(a), indicating that it is Mg_3Al–CO_3 LDH while only C can be detected in Fig. 6(b). The SEM-EDX elemental mappings of Mg and Al were performed with 9 wt% PP/Mg_3Al–CO_3 nanocomposites, as shown in Fig. 7, clearly indicating that the Mg_3Al–CO_3 LDH nanoparticles are well dispersed in PP.

3.3 Performance test of PP/LDH nanocomposites

Since LDH nanofillers may affect the thermal stability of PP, the influence of different anion intercalated LDHs on the thermal stability of PP was further studied by TGA, as shown in Fig. 8. The weight loss is observed to start after about 245 °C for all the samples. The temperature for 50% weight loss ($T_{0.5}$) of pure PP was 337 °C. The $T_{0.5}$ of PP/Mg_3Al–SO_4 LDH nanocomposites showed a slight decrease by *ca.* 5 °C. However, the $T_{0.5}$ of

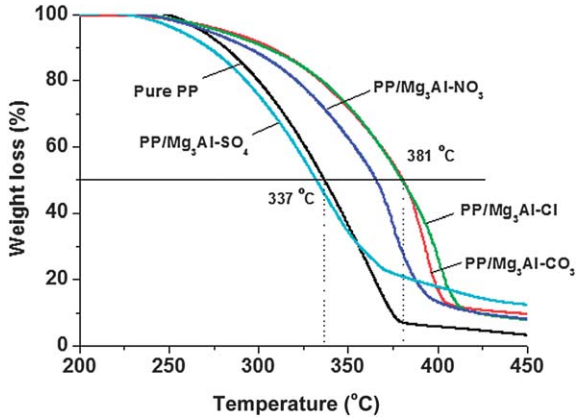

Fig. 8 TGA analysis of PP/Mg_3Al–X LDH nanocomposites with 9 wt% LDH loading.

Table 1 DSC analysis of pure PP and PP/Mg_3Al–X LDH nanocomposites with 9 wt% LDH loading

Nanocomposites	T_c/°C	ΔH_c/J g^{-1}	T_m/°C	ΔH_m/J g^{-1}	X_c (%)
Pure PP	108.31	85.61	153.65	85.70	58.44
PP/Mg_3Al_1–SO_4	119.43	81.38	158.33	85.54	55.55
PP/Mg_3Al_1–CO_3	121.27	87.94	157.98	89.37	60.03
PP/Mg_3Al_1–NO_3	118.17	89.09	156.56	93.74	60.81
PP/Mg_3Al_1–Cl	119.22	89.89	156.66	87.09	61.36

PP/Mg_3Al–CO_3, PP/Mg_3Al–NO_3, and PP/Mg_3Al–Cl LDH nanocomposites all significantly increased. Particularly with Mg_3Al–CO_3 and Mg_3Al–Cl LDHs, $T_{0.5}$ increased by about 44 °C compared to pure PP. Therefore, it can be easily concluded that the interlayer anions actually have a big effect on the thermal stability of the final PP/LDH nanocomposites. Regarding the thermal enhancement, CO_3^{2-} and Cl^- intercalated LDHs are preferred for PP nanocomposites.

The melting and recrystallisation behavior of the nanocomposites were studied by DSC. Table 1 shows the DSC data of pure PP and PP/Mg_3Al–X (CO_3^{2-}, NO_3^-, Cl^-, and SO_4^{2-}) LDH nanocomposites with 9 wt% LDH loading. The recrystallization temperature (T_c), melting temperature (T_m), melting enthalpy (ΔH_m), and degree of crystallinity (X_c) are summarized and listed in Table 1. ΔH_c and X_c are calculated using eqn (1).

$$X_c = (\Delta H_c/\Delta H_0) \times 100\% \quad (1)$$

where ΔH_0 is the melting enthalpy of the 100% crystalline PP, which is 146.5 J g^{-1}.[40] As can be seen from Table 1, the X_c of PP/Mg_3Al–SO_4 LDH nanocomposites decreased by *ca.* 2.89%. In contrast, PP/Mg_3Al–CO_3, PP/Mg_3Al–NO_3, PP/Mg_3Al–Cl LDH nanocomposites exhibited enhanced X_c by *ca.* 1.59%, 2.37%, and 2.92%, respectively, compared to pure PP. In addition, the incorporation of LDH is observed to increase T_m and T_c of PP by about 3–4 °C and 10–13 °C, respectively. On the other hand, the melting enthalpy (ΔH_m) increased by 3.67 J g^{-1}, 8.04 J g^{-1}, and 1.39 J g^{-1} after adding Mg_3Al–CO_3, Mg_3Al–NO_3, and Mg_3Al–Cl LDHs with 9 wt% loading, respectively.

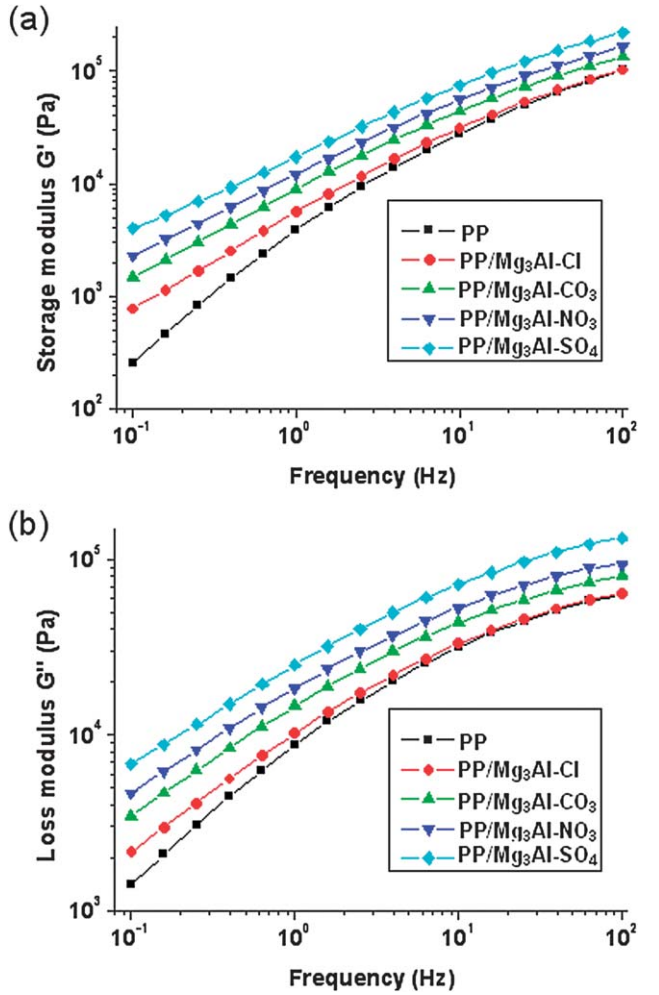

Fig. 9 (a) Storage modulus (G') and (b) loss modulus (G'') as a function of frequency for PP and PP/Mg_3Al–X LDH nanocomposites.

The rheological behavior of the nanocomposite melts is very important for industrial nanocomposite processing. The storage and loss moduli of the pure PP and PP/LDH nanocomposite melts are presented in Fig. 9, with a log–log plot as a function of angular frequency (ν). Both the storage modulus (G') and loss modulus (G'') of pure PP increased after introducing Mg_3Al–X LDHs, which results from a high surface friction of the PP/LDH interlayer. A similar phenomenon has been reported previously.[41] The influence on the storage and loss moduli follows the order of Mg_3Al–SO_4 > Mg_3Al–NO_3 > Mg_3Al–CO_3 > Mg_3Al–Cl, suggesting that different interlayer anions could result in different rheological properties.

Fig. 10(a) shows the mechanical loss factor (tan δ) as a function of w. tan δ is the ratio of loss modulus to storage modulus, which is highly related to the applied w. For pure PP, tan δ decreases monotonously with the increase in w. However, after adding LDHs, the tan δ of all PP/Mg_3Al–X nanocomposites starts to show three different stages: rubbery, viscoelastic and glassy states.[42] The tan δ of all nanocomposites decreased in the order of PP/Mg_3Al–SO_4 < PP/Mg_3Al–NO_3 < PP/Mg_3Al–CO_3 < Mg_3Al–Cl < PP. The incorporation of the LDH nanoparticles

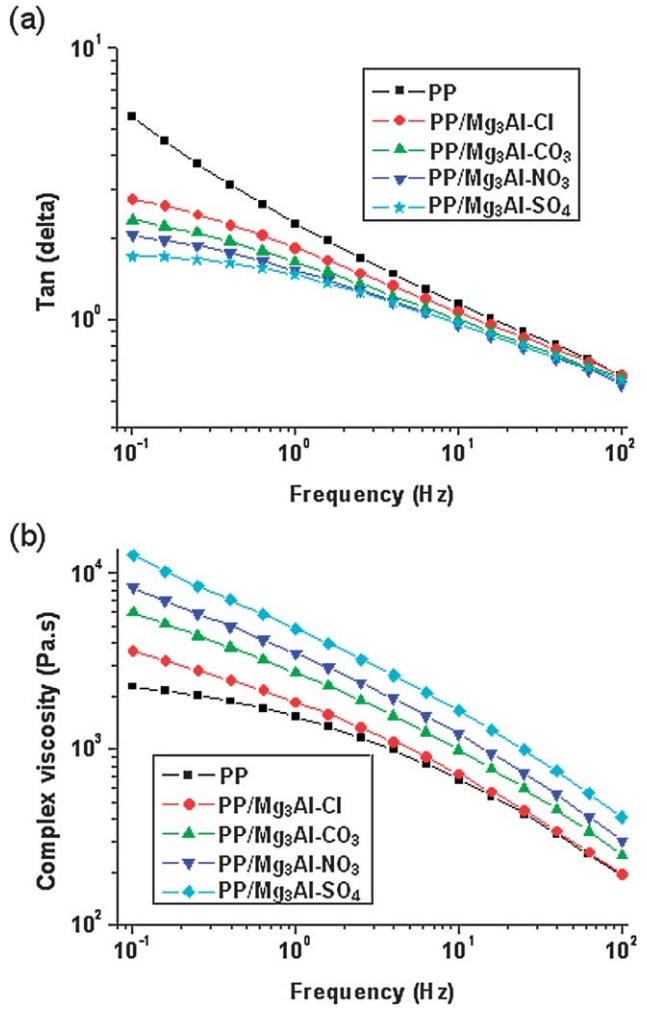

Fig. 10 (a) Mechanical loss factor (tan δ) and (b) complex viscosity (η^*) as a function of frequency for PP and PP/Mg_3Al–X LDH nanocomposites.

restrains the relative motion of the polymer chain and makes the nanocomposites "stiffer".[33,43–45]

Fig. 10(b) shows the complex viscosity (η^*) as a function of w for pure PP and its nanocomposite melts at 200 °C. $\eta^*(w)$ is strongly related to G' and G'' and can be calculated using eqn (2).

$$\eta^*(w) = [(G'/w)^2 + (G''w^2)]^{1/2} \quad (2)$$

The pure PP shows a classical viscoelastic behavior characterized by a transition from low frequency Newtonian flow behaviour to a high frequency shear thinning nature (viscosity decreases with an increase of shear rate/frequency).[46,47] However, after adding LDHs, the viscosity curves of all nanocomposites become linear within the whole frequency range. This phenomenon indicates the filler dominated fluid in the nanocomposites with 9 wt% LDH loading. The transition in η^* indicates that the nanocomposites have reached a rheological percolation, at which the nanoparticles form a network structure and greatly impede the motion of the polymer chains.[48] η^* of these PP/LDH nanocomposite melts increases in the order of PP/Mg_3Al–SO_4 > PP/Mg_3Al–NO_3 > PP/Mg_3Al–CO_3 > Mg_3Al–Cl > PP. The increment of the melt viscosity results from the stronger interaction between LDH with various LDH fillers and the PP matrix, indicating that LDH particles restrict the PP chain movements more significantly.

In summary, we have demonstrated that the interlayer anions have a big effect on the thermal stability, melting and recrystallisation behavior, and rheological property of PP. Considering that all LDHs have a similar layered structure and chemical composition, the intrinsic reason for the difference caused by the anions is still under investigation. One possible explanation might be that the different intercalation reactions give slightly different LDH particle sizes and size distributions, which dominates the physical and mechanical performance of the PP/LDH nanocomposites.

4 Conclusions

We reported for the first time four different inorganic anion (CO_3^{2-}, NO_3^-, Cl^-, and SO_4^{2-}) intercalated Mg_3Al LDHs as nanofillers and their influence on the thermal stability, melting and recrystallisation behavior and rheological property of PP. In order to improve the distribution of LDHs within the PP matrix, a solvent mixing method was used for the preparation of PP/LDH nanocomposites. XRD and SEM analyses indicated that LDH was successfully introduced into PP with a good dispersion. TGA analysis indicated that the thermal stability can be significantly improved, particularly with Mg_3Al–CO_3 and Mg_3Al–Cl LDHs, and the $T_{0.5}$ increased by 44 °C compared to pure PP. The melting and recrystallisation behavior of nanocomposites were studied by DSC, and the T_m and T_c of PP increased by 3–4 °C and 10–13 °C, respectively. In addition, the melting enthalpy (ΔH_m) increased by 3.67 J g^{-1}, 8.04 J g^{-1}, and 1.39 J g^{-1} after adding Mg_3Al–CO_3, Mg_3Al–NO_3, and Mg_3Al–Cl LDHs, respectively. The influence on the storage modulus (G') and loss modulus (G'') follows the order of Mg_3Al–SO_4 > Mg_3Al–NO_3 > Mg_3Al–CO_3 > Mg_3Al–Cl. The tan δ of all nanocomposites decreased with the order of PP/Mg_3Al–SO_4 < PP/Mg_3Al–NO_3 < PP/Mg_3Al–CO_3 < Mg_3Al–Cl < PP. The η^* of these PP/LDH nanocomposite melts increases in the order of PP/Mg_3Al–SO_4 > PP/Mg_3Al–NO_3 > PP/Mg_3Al–CO_3 > Mg_3Al–Cl > PP. The increment of the melt viscosity results from the stronger interaction between LDH with various LDH fillers and the PP matrix, indicating that LDH particles restrict the PP chain movements more significantly.

Acknowledgements

This work was supported by the Fundamental Research Funds for the Central Universities (TD-JC-2013-3), the Program for New Century Excellent Talents in University (NCET-12-0787), and Key Laboratory of Functional Inorganic Material Chemistry (Heilongjiang University), Ministry of Education.

References

1 J. H. Park, J. M. Ko, O. O. Park and D. W. Kim, *J. Power Sources*, 2002, **105**, 20.
2 L. Shao, S. Quan, X.-Q. Cheng, X.-J. Chang, H.-G. Sun and R.-G. Wang, *Int. J. Hydrogen Energy*, 2013, **38**, 5122.

3 L. Shao, C. Mu, H. Du, Z. Czech, H. Du and Y. Bai, *Appl. Surf. Sci.*, 2011, **258**, 1682.
4 C. Y. Kwong, W. C. H. Choy, A. B. Djurisic, P. C. Chui, K. W. Cheng and W. K. Chan, *Nanotechnology*, 2004, **15**, 1156.
5 Z. Guo, S. Park, H. T. Hahn, S. Wei, M. Moldovan, A. B. Karki and D. P. Young, *J. Appl. Phys.*, 2007, **101**, 09M511.
6 Z. Guo, S. E. Lee, H. Kim, S. Park, H. T. Hahn, A. B. Karki and D. P. Young, *Acta Mater.*, 2009, **57**, 267.
7 J. Zhu, S. Wei, M. J. Alexander, T. D. Dang, T. C. Ho and Z. Guo, *Adv. Funct. Mater.*, 2010, **20**, 3076.
8 J. Zhu, X. Zhang, N. Haldolaarachchige, Q. Wang, Z. Luo, J. Ryu, D. P. Young, S. Wei and Z. Guo, *J. Mater. Chem.*, 2012, **22**, 4996.
9 Y. Li, J. Zhu, S. Wei, J. Ryu, Q. Wang, L. Sun and Z. Guo, *Macromol. Chem. Phys.*, 2011, **212**, 2429.
10 S. Wei, P. Mavinakuli, Q. Wang, D. Chen, R. Asapu, Y. Mao, N. Haldolaarachchige, D. P. Young and Z. Guo, *J. Electrochem. Soc.*, 2011, **158**, K205.
11 M. Yamaguchi, H. Miyata and K. Nitta, *J. Appl. Polym. Sci.*, 1996, **62**, 87.
12 Q. Wang, X. Zhang, J. Zhu, Z. Guo and D. O'Hare, *Chem. Commun.*, 2012, **48**, 7450.
13 Q. Wang and D. O'Hare, *Chem. Rev.*, 2012, **112**, 4124.
14 Q. Wang, S. V. Y. Tang, E. Lestercd and D. O'Hare, *Nanoscale*, 2013, **5**, 114.
15 Q. Wang, H. H. Tay, D. J. W. Ng, L. Chen, Y. Liu, J. Chang, Z. Zhong, J. Luo and A. Borgna, *ChemSusChem*, 2010, **3**, 965.
16 Q. Wang, Y. Gao, J. Luo, Z. Zhong, A. Borgna, Z. Guo and D. O'Hare, *RSC Adv.*, 2013, **3**, 3414.
17 Q. Wang, H. H. Tay, Z. Guo, L. Chen, Y. Liu, J. Chang, Z. Zhong, J. Luo and A. Borgna, *Appl. Clay Sci.*, 2012, **55**, 18.
18 Q. Wang, J. Yu, J. Liu, Z. Guo, A. Umar and L. Sun, *Sci. Adv. Mater.*, 2013, **5**, 469.
19 Q. Wang, Y. Gao, Z. Zhang, L. Duan, A. Umar and D. O'Hare, *Sci. Adv. Mater.*, 2013, **5**, 411.
20 V. Rives, *Layered Double Hydroxides: Present and Future*, Nova Science, 2001.
21 Y. Zhao, M. Wei, J. Lu, Z. Wang and X. Duan, *ACS Nano*, 2009, **3**, 4009.
22 Y. Lin, D. Li, D. G. Evans and X. Duan, *Polym. Degrad. Stab.*, 2005, **88**, 286.
23 Z. Xu, S. K. Saha, P. S. Braterman and N. D. Souza, *Polym. Degrad. Stab.*, 2006, **91**, 3237.
24 D. G. Evans and X. Duan, *Chem. Commun.*, 2006, 485.
25 Q. Wang, H. H. Tay, L. Chen, Y. Liu, J. Chang, Z. Zhong, J. Luo and A. Borgna, *J. Nanoeng. Nanomanuf.*, 2011, **1**, 298.
26 D. Li, Z. Tuo, D. G. Evans and X. Duan, *J. Solid State Chem.*, 2006, **179**, 3114.
27 Y. Feng, D. Li, Y. Wang, D. G. Evans and X. Duan, *Polym. Degrad. Stab.*, 2006, **91**, 789.
28 X. Zhao, F. Zhang, S. Xu, D. G. Evans and X. Duan, *Chem. Mater.*, 2010, **22**, 3933.
29 C. Jiao, Z. Wang, X. Chen and Y. Hu, *J. Appl. Polym. Sci.*, 2008, **107**, 2626.
30 F. R. Costa, U. Wagenknecht and G. Heinrich, *Polym. Degrad. Stab.*, 2007, **92**, 1813.
31 Z. Cui and B. Qu, *Chin. J. Polym. Sci.*, 2010, **28**, 563.
32 L. Du and B. Qu, *J. Mater. Chem.*, 2006, **16**, 1549.
33 Q. Wang, X. Zhang, C. J. Wang, J. Zhu, Z. Guo and D. O'Hare, *J. Mater. Chem.*, 2012, **22**, 19113.
34 C. Nyambo, P. Songtipya, E. Manias, M. M. Jimenez-Gasco and C. A. Wilkie, *J. Mater. Chem.*, 2008, **18**, 4827.
35 C. M. Becker, A. D. Gabbardo, F. Wypych and S. C. Amico, *Composites*, 2011, **42**, 196.
36 W. Chen and B. Qu, *J. Mater. Chem.*, 2004, **14**, 1705.
37 D. Wang, A. Leuteritz, Y. Wang, U. Wagenknecht and G. Heinrich, *Polym. Degrad. Stab.*, 2010, **95**, 2474.
38 L. Shi, D. Li, S. Li, J. Wang, D. G. Evans and X. Duan, *Chin. Sci. Bull.*, 2005, **50**, 1101.
39 S. Xu, L. Zhang, Y. Lin, R. Li and F. Zhang, *J. Phys. Chem. Solids*, 2012, **73**, 1514.
40 S. P. Lonkar, S. Morlat-Therias, N. Caperaa, F. Leroux, J. L. Gardette and R. P. Singh, *Polymer*, 2009, **50**, 1505.
41 J. Zhu, S. Wei, Y. Li, L. Sun, N. Haldolaarachchige, D. P. Young, C. Southworth, A. Khasanov, Z. Luo and Z. Guo, *Macromolecules*, 2011, **44**, 4382.
42 G. Schramm, *A Practical Approach to Rheology and Rheometry*, Gebrueder HAAKE GmbH, Karlsruhe, Federal Republic Germany, 2nd edn, 2000.
43 Y. Li, J. Zhu, S. Wei, J. Ryu, L. Sun and Z. Guo, *Macromol. Chem. Phys.*, 2011, **212**, 1951.
44 X. Chen, S. Wei, A. Yadav, R. Patil, J. Zhu, R. Ximenes, L. Sun and Z. Guo, *Macromol. Mater. Eng.*, 2011, **296**, 434.
45 J. Zhu, S. Wei, Y. Li, L. Sun, N. Haldolaarachchige, D. P. Young, C. Southworth, A. Khasanov, Z. Luo and Z. Guo, *Macromolecules*, 2011, **44**, 4382.
46 A. J. Poslinski, M. E. Ryan, R. K. Gupta, S. G. Seshadri and F. J. Frechette, *J. Rheol.*, 1988, **32**, 703.
47 V. M. Ugaz, D. K. Cinader and W. R. Burghardt, *Macromolecules*, 1997, **30**, 1527.
48 A. V. Shenoy, *Rheology of Filled Polymer Systems*, Kluwer Academic Publishers, Dordrecht, The Netherlands, 1999.

